

Microfluidic filament thinning of aqueous, fibrillar methylcellulose solutionsAthena E. Metaxas ¹, McKenzie L. Coughlin ¹, Clayton K. Hansen ², Frank S. Bates ¹,
Timothy P. Lodge ^{1,3} and Cari S. Dutcher ^{1,2,*}¹*Department of Chemical Engineering and Materials Science, University of Minnesota – Twin Cities, 421 Washington Avenue SE, Minneapolis, Minnesota 55455, USA*²*Department of Mechanical Engineering, University of Minnesota – Twin Cities, 111 Church Street SE, Minneapolis, Minnesota 55455, USA*³*Department of Chemistry, University of Minnesota – Twin Cities, 207 Pleasant Street SE, Minneapolis, Minnesota 55455, USA*(Received 20 January 2020; accepted 21 September 2020;
published 6 November 2020)

Methylcellulose (MC), a methoxy-substituted cellulose ether, is widely used as a rheology modifier, binder, and water-retention agent in a variety of food, pharmaceutical, construction, and consumer applications. While soluble in water at low temperatures, MC reversibly transitions to a turbid hydrogel upon heating or upon the addition of NaCl, due to the formation of a fibrillar network. These complex MC solutions and gels experience a range of flow conditions in industrial processes, including shear and extensional flows. While the shear rheological behavior has been well characterized for many MC solutions, the extensional rheological behavior is often more challenging to characterize, particularly for solutions with lower molecular weights, relaxation times, and viscosities. Filament stretching using a flow-focusing microfluidic device is a promising method to resolve extensional properties of lower molecular weight and lower viscosity polymeric solutions, and it is used here to characterize MC solutions at varying NaCl concentrations. The flow-driven apparent extensional viscosity can be calculated from transient filament diameter thinning behavior of 1 wt% MC with a molecular weight of 150 kg/mol. The apparent extensional viscosity increased as the concentration of NaCl increased, from 0.947 ± 0.005 Pa s to 15.1 ± 0.6 Pa s between 0 and 8 wt% NaCl, respectively. The increase in apparent extensional viscosity is attributed to the presence of fibrils in the MC solutions containing NaCl annealed at room temperature, as demonstrated with cryogenic transmission electron microscopy. The study of the extensional behavior of this commercially relevant polymer should enable new ways to process MC, such as fiber spinning and extrusion.

DOI: [10.1103/PhysRevFluids.5.113302](https://doi.org/10.1103/PhysRevFluids.5.113302)**I. INTRODUCTION**

Extensional flow fields observed in nozzles and contracting channels are relevant in many industrial applications, including printing, fiber spinning, extrusion, coatings, spraying, and film blowing [1–6]. However, establishing the non-Newtonian behavior of fluids in extensional flow fields can be challenging, especially for low-viscosity, weakly elastic solutions. The information obtained from the thinning and progressive breakup of an initially stable fluid filament with time is a key method to studying these complex flows for droplets [7,8], emulsions [9–11], and polymer solutions [12–15]. For example, a typical macroscale method for determining extensional properties

*cdutcher@umn.edu

of polymer solutions is Capillary Break-up Extensional Rheology (CaBER), where a step-strain is applied to a fluid or semisolid between two parallel plates, and the fluid filament flows and thins due to a balance between viscous and/or elastic stresses and capillary action. The diameter of the thinning filament is measured as a function of time by a laser housed in the device or by image analysis with a high-speed camera, where properties such as extensional relaxation time and extensional viscosity can be extracted from relevant constitutive equations. Although convenient, CaBER only reliably determines these properties of solutions with shear viscosities above 100 mPa s, as lower viscosity solutions tend to break up before relevant quantitative information can be collected [16–18].

Microfluidic flow-focusing devices, such as the device used by Arratia *et al.* [19,20], are much smaller in scale than the CaBER. Combined with high-speed imaging, flow-focusing devices offer a potential solution to the drawbacks associated with CaBER. Because the ratio of elastic to inertial forces, defined as the elasticity number $El = \lambda\eta_s/(\rho l)^2$, where λ is the relaxation time, η_s is the solution shear viscosity, and ρ is the fluid density, scales with the inverse square of the characteristic length scale of a device, l , the viscoelastic behavior of a polymer solution can be enhanced in a microfluidic device [21]. The range of measurable extensional strain rates in a microfluidic device is also extended by several orders of magnitude from those accessible by CaBER [22–27]. In addition, the presence of an oil phase surrounding the thinning filament can help regulate temperature and suppress evaporation, as those can also be concerns in a method such as CaBER. Finally, the microfluidic device setups also require very small volumes of solution and are high throughput, providing large datasets from small sample amounts.

The extensional behavior of methylcellulose (MC) is of interest due to processing that involves extensional deformation. Methylcellulose is used as a rheology modifier in a variety of food, pharmaceutical, and consumer product industries because of its unique properties. MC is a cellulose derivative partially substituted with methoxy groups (on average 1.7–2.2 out of 3 hydroxyl groups per anhydroglucose unit), which renders it soluble in water at temperatures below about 50 °C [28]. In addition to its solubility in water at lower temperatures, MC can reversibly transition to a turbid hydrogel upon heating or with the introduction of NaCl into solution around room temperature [29,30]. The current consensus for the thermoreversible gelation mechanism involves the formation of MC fibrils. Extensive work using cryogenic transmission electron microscopy (cryo-TEM), rheological measurements, and small-angle X-ray and neutron scattering (SAXS and SANS) support the hypothesis that the fibrillar network is responsible for the mechanical response of this material [31–35].

Prior studies have successfully vitrified MC solutions after annealing above the gel point in solutions that did not contain salt. Cryo-TEM images obtained from these glassy thin films showed fibrils with an average diameter of ~ 15 nm, which was further corroborated by SAXS and SANS on these solutions [31,34–36]. Simulations in recent years support the proposal that the fibrils are composed of a core of axially oriented chains with polymer chains wrapped around the core to form twisted bundles, which are formed by chain bending and water-mediated interchain interactions [37–40]. A recent experimental study using SAXS, medium- and wide-angle X-ray scattering (MAXS and WAXS) on oriented gel samples confirms that the average chain axis is oriented along the fibril axis and that the fibrils include crystalline regions [41].

While the shear behavior of methylcellulose solutions has been extensively studied, the extensional behavior of this polymer has not, until a study by Morozova *et al.* [42] examined the extensional behavior of MC solutions using CaBER as a function of MC concentration and NaCl concentration. The study found that the presence of NaCl resulted in an elastocapillary regime, from which the extensional relaxation time and apparent extensional viscosity were calculated from Hencky strains ranging from 1.5 to 5. The emergence of this elastocapillary regime was attributed to the formation of fibrils in solution at room temperature. Unfortunately, CaBER can only reliably resolve MC solutions with molecular weights of 250 kg/mol and higher, as shown in Fig. S1 in the Supplemental Material [43], as lower molecular weight samples have viscosities and relaxation times that render the CaBER technique ineffective.

Recently, Micklavzina *et al.* [44] used hyperbolic microfluidic contractions to extend the range of extensional rheology measurements of MC solutions to lower viscosities, and resolved extensional viscosities between 0.01 and 1 Pa s using pressure drop measurements. However, a drawback of the single-phase contraction channel is the dominant contribution of viscous losses in the contraction [45,46]. Here, we couple the advantage of MC solution filament thinning by the surrounding outer fluid extensional flow with the advantage of the improved strain-rate range accessible in microfluidic devices. In this study, the extensional properties of MC solutions over a range of NaCl concentrations were examined using microfluidic flow-focusing devices to generate dynamically thinning filaments. The work discussed here presents a relatively straightforward method to obtain extensional properties that were previously unattainable to expand the understanding of MC behavior under extensional flow fields.

II. MATERIALS AND METHODS

A. Methylcellulose solution preparation

Methylcellulose ($M_w \approx 150$ kg/mol, $D \approx 3.6$, degree of methoxy group substitution, $DS \approx 1.8$) was provided by The Dow Chemical Company. NaCl was American Chemical Society (ACS) grade from Fisher Scientific and was used as received. MC was dried under vacuum (~ 100 mTorr) at 50°C for 24 h to eliminate any excess water. The concentration of MC for all solutions in this study was 1 wt%, which for MC150 in water is approximately five times the overlap concentration c^* of 0.21 wt% [32,47]. To prepare the solutions, 0.5 g of MC was dissolved in 25 g of High Performance Liquid Chromatography (HPLC) grade chromatography water (Fisher Scientific) at 60°C and stirred for 10 min in a 50 mL glass jar. For solutions that contained NaCl, 1 g (2 wt%), 2.5 g (5 wt%), or 4 g (8 wt%) were dissolved with the MC in water at 60°C . The remaining quantity of water at room temperature ($\sim 23^\circ\text{C}$) was added to yield a total solution weight of 50 g and stirred for an additional 10 min. The solutions were placed into an ice bath, stirred for 10 min, and then stored in a refrigerator at 2°C for at least 24 h. These samples can be used for up to a month after preparation. The solutions were annealed at room temperature for 24 h prior to any measurements using cryo-TEM, steady shear and oscillatory rheology, or microfluidic filament thinning.

B. Steady shear and oscillatory shear rheology

Shear and oscillatory rheology experiments were conducted on a TA Instruments AR-G2 rheometer. For steady-shear experiments, a 2° steel 40-mm cone and Peltier plate geometry was used. The shear viscosity for each 1 wt% MC solution (with 0, 2, 5, or 8 wt% NaCl) was measured after the torque signal reached a steady state for shear rates ranging from 0.1 to 5000 s^{-1} . The temperature was kept constant at 23°C for all experiments. Oscillatory shear experiments were taken using a cup and bob geometry (rotor o.d. 14 mm, rotor height 42 mm, cup i.d. 15 mm, and gap height 5 mm) from 0 to 80°C and 80 to 0°C at a temperature ramp rate of $1^\circ\text{C}/\text{min}$ at 1% strain amplitude with an angular frequency of 1 rad/s .

C. Cryo-TEM

NaCl-free and 8 wt% NaCl solutions of 0.1 wt% MC were prepared as described in Sec. A. To vitrify the samples, an FEI Vitrobot Mark IV vitrification system was used with the climate control chamber set to 25°C and 100% humidity. Lacy carbon/Formvar grids (Ted Pella, 300 mesh) were cleaned and hydrophilized using a PELCO easiGlow discharge cleaning system. Five μL of each sample were pipetted onto separate grids, and the grids were annealed in the Vitrobot chamber for 1 s before the grid was blotted for 1 s with a blot force set to -1 , equilibrated for 1 s, and plunged into liquid ethane cooled by liquid nitrogen. The vitrified grids were stored in liquid nitrogen prior to imaging. The sample grids were transferred to a Gatan-626 single-tilt cryo-holder and imaged using an FEI Tecnai G2 Spirit BioTWIN microscope operated at 120 kV coupled with an FEI Eagle

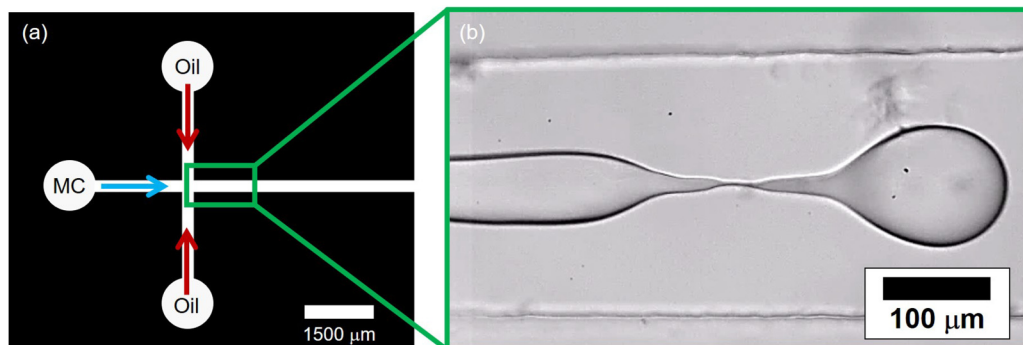


FIG. 1. (a) Schematic of the microfluidic flow-focusing device. The MC solution flows through the leftmost entrance port and is surrounded by a continuous phase of 50 cSt silicone oil. (b) A movie at 20,000 fps is recorded to capture the filament thinning behavior as shown. Edge detection is then applied to obtain the filament diameter with time.

charge-coupled device camera (2048×2048 pixels). Images were obtained from multiple areas of the grid to determine if fibrils were formed in the MC solutions.

D. Extensional filament thinning in microfluidic devices

The microfluidic device for extensional filament thinning measurements was fabricated using standard soft-lithography techniques described extensively in the literature [48–50]. A photolithography mask of the flow-focusing device was drawn using 2D CAD software (DRAFTSIGHT) and printed on a 20,000-dpi high-resolution printer (CAD/Art Services, Inc.), as shown in Fig. 1(a). In the clean room, a blank silicon wafer was cleaned using a piranha solution and spin coated with a negative photoresist (SU-8 2050, Microchem). After a preexposure bake, a mask aligner (Karl Süss) was used to expose the photoresist to UV light and developed to form an SU-8 mold of the flow-focusing device. Prior to pouring poly(dimethylsiloxane) (PDMS, SYLGARD 184 silicone elastomer, 10:1 elastomer to crosslinker ratio, Dow Corning Corporation), the surface of the mold was rinsed with isopropanol, dried with compressed air, and treated with silanes [(tridecafluoro-1,1,2,2-tetrahydrooctyl)trichlorosilane, Gelest] to allow for easy removal of the PDMS device from the surface of the silicon wafer. Approximately 20 μL of the silanes were pipetted into a watchglass and placed with the cleaned wafer into a desiccator and held for 20 min under vacuum.

After treating the wafer surface, the PDMS was poured onto the mold and baked overnight at 70 $^{\circ}\text{C}$ to allow the PDMS to harden. To seal the bottom of the PDMS device and mitigate wetting effects, a glass coverslip was spin coated with PDMS and allowed to bake overnight. The device was then cut out from the mold and holes were punched into the three inlets [two side arms for the continuous silicone oil phase, one central arm for the MC solution, and one outlet as shown in Fig. 1(a)] using a 0.75-mm-o.d. biopsy punch (World Precision Instruments). The PDMS device and PDMS-coated glass coverslip were rinsed with methanol, isopropanol, distilled water, and dried with compressed air. The device and coverslip were plasma treated (Harrick Plasma), sealed, and baked for a minimum of 2 h in an oven at 70 $^{\circ}\text{C}$ to render the channel walls hydrophobic and prevent the aqueous MC solutions from adhering to the walls. The device channel width is 250 μm while the device channel height is 120 μm , which was confirmed with optical microscopy and IMAGEJ.

The device was then mounted to the stage of an inverted microscope (Olympus IX73) for bright-field imaging using a 20 \times objective lens. Pressure-driven flow was generated using syringe pumps (Harvard Apparatus) with gas-tight glass syringes connected to perfluoroalkoxy tubing (PFA, inside diameter 0.02 in, outside diameter 0.0625 in, IDEX Corporation) and curved needles hermetically sealed to the device inlets and outlet. The continuous phase of 50 cSt silicone oil (Fisher Scientific)

TABLE I. Summary of relevant parameters for shear and extensional rheological characterization of MC solutions. The error for the flow behavior index is from the power-law fit, and the errors for the extensional viscosity and Trouton ratio represent a 95% confidence interval. The Trouton ratio was calculated for each sample at a Hencky strain of 0.1 with the method discussed using Eq. (6).

NaCl Conc. (wt%)	Flow behavior index, n	Dispersed phase volumetric flow rate, Q_d (cm ³ /min)	Continuous phase volumetric flow rate, Q_c (cm ³ /min)	Flow-driven extensional viscosity, η_e (Pa s)	Trouton ratio
0	0.831 ± 0.007	0.008	0.015	0.947 ± 0.005	26.9 ± 0.3
2	0.821 ± 0.006	0.008	0.015	1.62 ± 0.01	40.5 ± 0.3
5	0.793 ± 0.006	0.008	0.050	2.7 ± 0.4	56 ± 13
8	0.446 ± 0.009	0.008	0.600	15.1 ± 0.6	271 ± 35

was pumped in at a specified volumetric flow rate (see Table I) and allowed to flow through the device for several minutes prior to pumping in the MC solution. The silicone oil is Newtonian, as confirmed by steady-shear measurements. The dispersed phase flow rate was held constant at 0.008 cm³/min for all MC solutions. The field of view was adjusted near the cross junction to record movies at 20 000 frames per second (fps) on a Photron FASTCAM Mini UX100 high-speed camera. A frame from a sample movie is shown in Fig. 1(b).

Once the movies were recorded, they were processed in MATLAB using an in-house code to apply an intensity threshold to the interface between the continuous, silicone oil phase and the dispersed, aqueous 1 wt% MC150 solution phase. Sample movie frames with applied thresholding for the solution containing 0 wt% NaCl are shown in Fig. 2(b). Sample movie frames from the three other solutions (2, 5, and 8 wt% NaCl) can be found in the Supplemental Material (Figs. S2–S4) [43]. The filament diameter, $D(t)$, can be calculated in terms of pixels for each frame of the movie and converted to a μm length scale since the channel width is known. The filament diameter measurements were collected at five user-defined locations in an Eulerian frame, as represented by the vertical white lines in Fig. 2(b). The transient region as the drop passes occurs at times less than 10 ms, and this is not used in the calculation. In contrast, for times over 10 ms, the thinning behavior is nearly identical across the region of interest, regardless of where the image analysis is performed within the thinning region shown. The orange, dashed box shown in Fig. 2(a) shows the portion of the trace that is used for extensional viscosity calculations as the filament diameters are below the channel height and therefore not in a confined state. Multiple filament break-up events were further analyzed to calculate extensional strain rate and flow-driven extensional viscosity, to be discussed later. Repeat runs for each solution can be found in Fig. S5 in the Supplemental Material [43].

III. RESULTS AND DISCUSSION

A. Shear rheology of aqueous methylcellulose solutions

The viscoelastic properties of MC150 solutions as a function of temperature and NaCl concentration were measured using small-amplitude oscillatory shear. Solutions of 1 wt% MC150 at NaCl concentrations ranging from 0 to 8 wt% were heated from 0 to 80 °C and back at a temperature ramp rate of 1 °C/min. Figure 3 shows that all MC150 solutions at varying NaCl concentrations undergo a sol-gel transition upon heating, as signified by the large increase in magnitude of the complex modulus, $|G^*|$. This is followed by a gel-sol transition upon cooling, as reflected in the large decrease in magnitude of $|G^*|$. These drastic changes in the complex modulus are attributed to the formation of MC fibrils upon heating and their dissolution upon cooling, indicating that the process is thermoreversible, albeit with substantial hysteresis [32,33].

The addition of NaCl decreases both the gel temperature (T_{gel}), which is taken as the midpoint of the overall sharp increase in the complex modulus upon heating, and the sol temperature (T_{sol}),

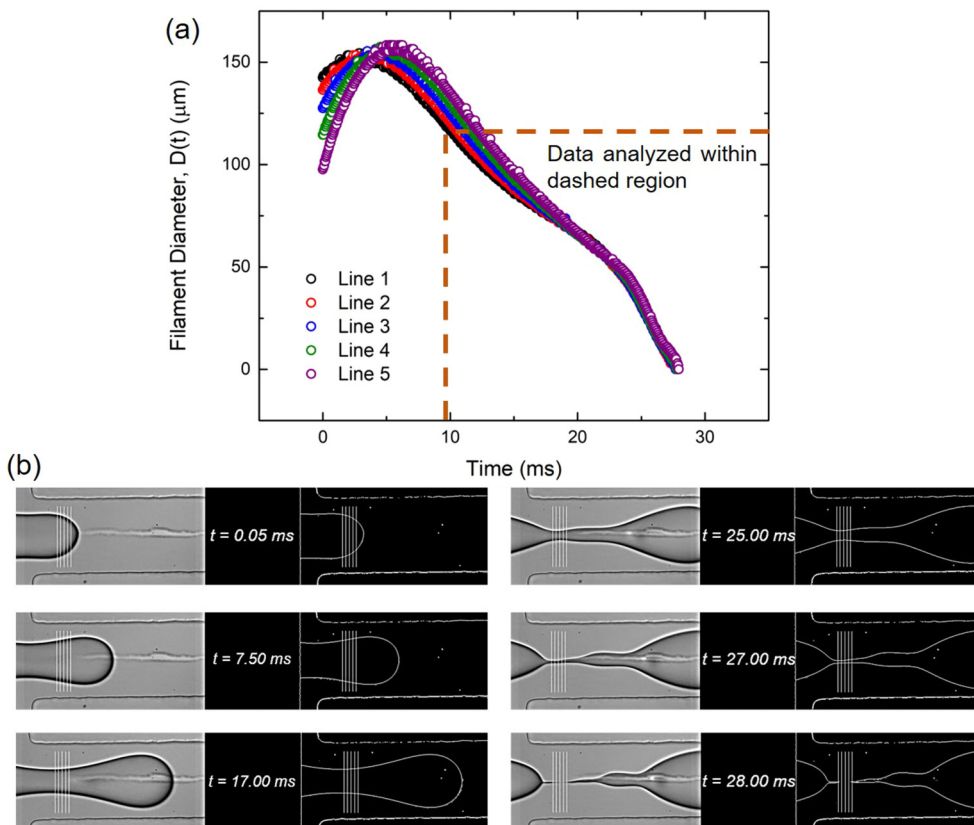


FIG. 2. (a) Filament diameter of the fluid front for 1 wt% MC150 in 0 wt% NaCl passing through all five white, vertical lines in the snapshots of a sample movie shown in (b). The raw movie frame is on the left-hand side of each column while the frame with applied thresholding is shown on the right-hand side of each column in (b). The vertical white lines indicate where the filament diameter, $D(t)$, can be measured. The channel width is $250 \mu\text{m}$ in all frames shown here. The area boxed in with the orange dashed lines indicates the region where the data were analyzed, described in the Results and Discussion.

taken here as the midpoint of the sharp decrease in the complex modulus upon cooling, which is attributed to the transition of MC fibrils to dissolved chains. With sufficient NaCl, fibrils can be formed at lower temperatures. Indeed, there is a $\sim 30^\circ\text{C}$ difference between the sol-gel and gel-sol transitions between the two extreme NaCl concentrations. The gel-sol transition, which is the lower temperature limit for fibril formation, is at or below room temperature for the 5 and 8 wt% NaCl solutions [35]. This behavior is consistent with what was observed for higher molecular weight MC solutions [36,42]. One aspect to note is that even at the highest concentration of NaCl, the solution still flows freely as the yield stress is only around 1 Pa as shown in Fig. S6 in the Supplemental Material [43]. This ability for the MC solutions to flow freely is imperative for pumping the solution through the microfluidic filament thinning device to maintain a Reynolds number, Re , of less than 1.

The steady-shear behavior of the 1 wt% MC150 solutions is also modified by the presence of fibrils to varying degrees depending upon the NaCl concentration in solution. The shear viscosity as a function of shear rate at room temperature (23°C) for each solution is shown in Fig. 4. The shear thinning observed at higher shear rates $> 250 \text{ s}^{-1}$ in all solutions is similar to what was observed at higher molecular weights of MC and is attributable to free (nonfibrillar) MC chains [45]. Similar

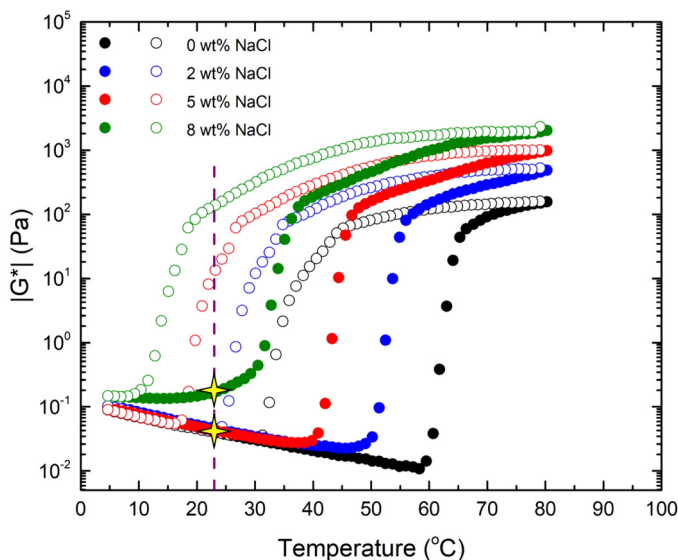


FIG. 3. Complex moduli for 1 wt% MC150 solutions in 0, 2, 5, and 8 wt% NaCl at 1% strain, 1 rad/s, and heating and cooling rates of 1 °C/min. The filled and open symbols refer to heating and cooling traces, respectively. The purple, dashed line denotes the operating temperature of all microfluidic filament-thinning experiments (23 °C). The MC solutions for the filament-thinning experiments were removed from the refrigerator and allowed to warm to 23 °C (room temperature), thus falling on the heating trace as indicated by the yellow stars.

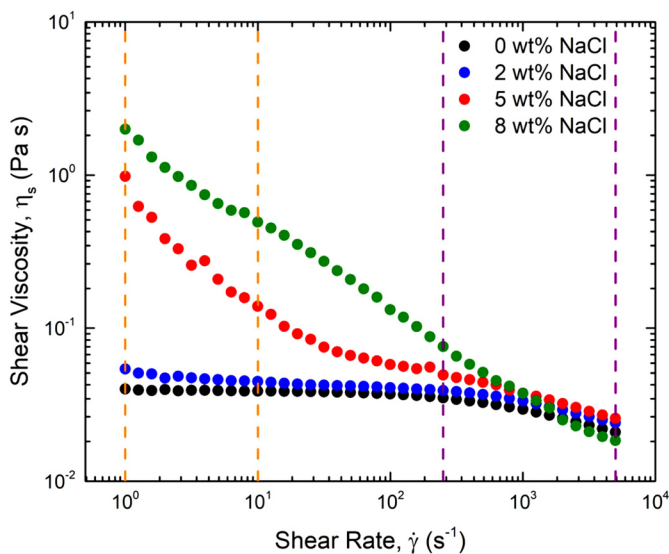


FIG. 4. Steady-shear viscosity as a function of shear rate for 1 wt% MC150 solutions in 0, 2, 5, and 8 wt% NaCl at 23 °C. Two shear-thinning regions separated by the vertical, dashed lines are present in the traces with NaCl: one at lower shear rates due to the shear-thinning effects of the fibrils (orange, dashed lines) and one at higher shear rates due to the shear-thinning effects of MC coils in solution (purple, dashed lines).

behavior has also been observed by Dinic and Sharma [51] in another cellulose ether analog, hydroxyethyl cellulose. At these higher shear rates, the shear viscosity decreases, and the flow behavior index, n , can be determined by fitting the higher shear rate values from 250 to 5000 s^{-1} :

$$\eta_s = K\dot{\gamma}^{n-1}, \quad (1)$$

where η_s is the shear viscosity, K is the flow consistency index, and $\dot{\gamma}$ is the shear rate. The flow behavior index decreases with increasing NaCl concentration, where $n = 0.831 \pm 0.007$, 0.821 ± 0.006 , 0.793 ± 0.006 , and 0.446 ± 0.009 for 0 to 8 wt% NaCl, respectively, as reported in Table I. The power-law fits can be seen in Fig. S7 of the Supplemental Material [43]. The decreasing values of n indicate more shear thinning with increasing NaCl concentration. At lower shear rates, the shear viscosity of the 0 wt% NaCl asymptotes to give a zero-shear viscosity of 0.05 Pa s. The shear viscosity behavior for the MC150 solutions containing NaCl, however, is not constant with shear rate. A second “shear-thinning” regime is observed at lower shear rates (below 200 s^{-1}), attributed to the presence of fibrils. These differences in shear-thinning behavior across the solutions will become important in the last section where the extensional rheological behavior of these solutions is discussed.

B. Visualization of methylcellulose fibrils annealed at room temperature

As previously noted, the formation of MC fibrils is responsible for the onset of gelation and the mechanical response of these samples. While the shear behavior suggests that intermolecular association occurs to give the response seen in Figs. 3 and 4, it cannot produce a direct measure of the fibril structure. Cryogenic transmission electron microscopy was therefore used to directly image the fibril structure [31,33]. Here, the occurrence of MC fibrils in the presence of NaCl for systems annealed at room temperature for 24 h prior to vitrification was verified. Figure 5(a) depicts a cryo-TEM image of 0.1 wt% MC150 solution with 0 wt% NaCl. As expected from the location of the sol-gel and gel-sol temperatures in Fig. 3 and the shear behavior in Fig. 4, no fibrils are present. Figure 5(b) depicts a cryo-TEM image of 0.1 wt% MC150 solution in 8 wt% NaCl, where variations in contrast in the form of darker cylindrical objects, which are MC fibrils, can be seen against the lighter substrate. As documented in a prior study by Schmidt *et al.* [36], the average fibril diameter remains constant regardless of molecular weight or concentration of MC, but it does change with the amount of salt in solution. Because the fibrils contain water, the presence of NaCl increases the osmotic pressure, which ultimately extracts the water and therefore decreases the filament diameter from approximately 15 nm from prior SAXS and IMAGEJ analysis of cryo-TEM images to 11 nm using IMAGEJ analysis in this study. Similar behavior has been observed in other gel systems, where the presence of dissolved ions decreases the diameter of the respective structures [52–54].

C. Filament thinning of aqueous methylcellulose to measure extensional viscosity

The filament thinning profiles of the MC solutions in the microfluidic devices generated from the movies are shown in Fig. 6(a) in terms of filament diameter, $D(t)$, as a function of time. As the NaCl concentration increased, the MC solution viscosity increased as shown in Fig. 4, which required higher volumetric flow rates of the continuous silicone oil phase to form a filament, as shown in Table I. This accounts for the progressively shorter break-up times as the NaCl concentration increased [27]. The volumetric flow rate for the dispersed aqueous MC150 phase remained constant for all experiments. Note that all flows are maintained in the laminar flow regime, as the Reynolds numbers range from $Re = 0.012$ at the lowest continuous phase flow rate to $Re = 0.48$ at the highest continuous phase flow rate. With this particular geometry, there is no dependence on the evolution of $D(t)$ with axial position as seen in Fig. 2 and Figs. S2–S4 [20,43].

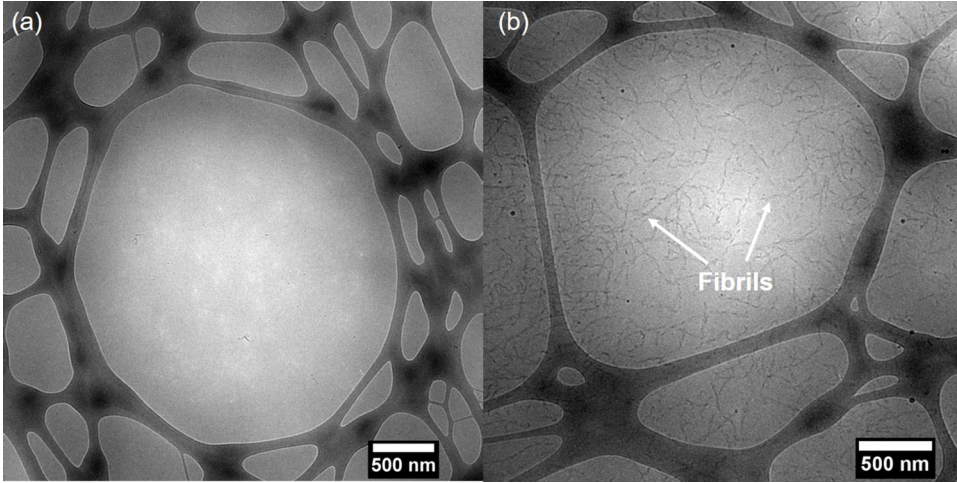


FIG. 5. Cryo-TEM images of 0.1 wt% MC solutions in (a) HPLC-grade water and (b) 8 wt% NaCl annealed at 23 °C for 24 h. Fibrils, denoted by the arrows, are only present for solutions with added NaCl at room temperature. The fibril diameters were measured using IMAGEJ to obtain an average diameter of 11 ± 1 nm.

From the filament diameter data, the extensional strain rate of the filament can be calculated by the following relationship:

$$\dot{\varepsilon} = -\left(\frac{2}{D(t)}\right)\left(\frac{dD(t)}{dt}\right), \quad (2)$$

where $D(t)$ is the filament diameter, t is time, and $\dot{\varepsilon}$ is the extensional strain rate of the MC filament. This form of extensional strain rate assumes that the filament is homogeneous in the axial direction [55,56]. Realistically, there is some variation in the filament diameter in the axial direction that would require an additional term to calculate the extensional strain rate. However, in these experiments, the local spatial rate of change in filament thickness is much smaller than the temporal rate of change, so the additional term can be neglected. To a good approximation, the filament can be treated as spatially uniform and Eq. (2) can be used to calculate the extensional strain rate, as seen in Fig. 6(b) [20].

Figure 6(b) shows that the extensional strain rate is initially independent of time, before sharply increasing by orders of magnitude. Both regimes (“flow-driven” filament thinning, where the extensional strain rate is constant with time, and “capillary-driven” filament thinning, where the extensional strain rate rapidly changes with time) contain information about the extensional viscosity of the solutions. In this regime, the filament diameter thins exponentially with time as seen in Fig. 6(a). Because the filament thinning is driven by the continuous phase (silicone oil) viscous stresses normal to the dispersed phase (MC solution) and the pressure drag imparted by the droplet at the end of a thinning filament, a stress balance can be calculated across the interface between the two phases

$$\eta_e \dot{\varepsilon} = \eta_{e,oil} \dot{\varepsilon}_{oil} + \frac{F_{drag}}{\pi \left(\frac{D(t)}{2}\right)^2}, \quad (3)$$

where the left-hand side represents the extensional stress of the MC solution and includes the extensional viscosity, η_e . The first term on the right-hand side represents the viscous stress the silicone oil applies to the MC solution, and the second term on the right-hand side represents the reactive force acting on the filament due to the pressure drag exerted by the oil on the confined leading droplet, defined later with Eq. (5) [4,57].

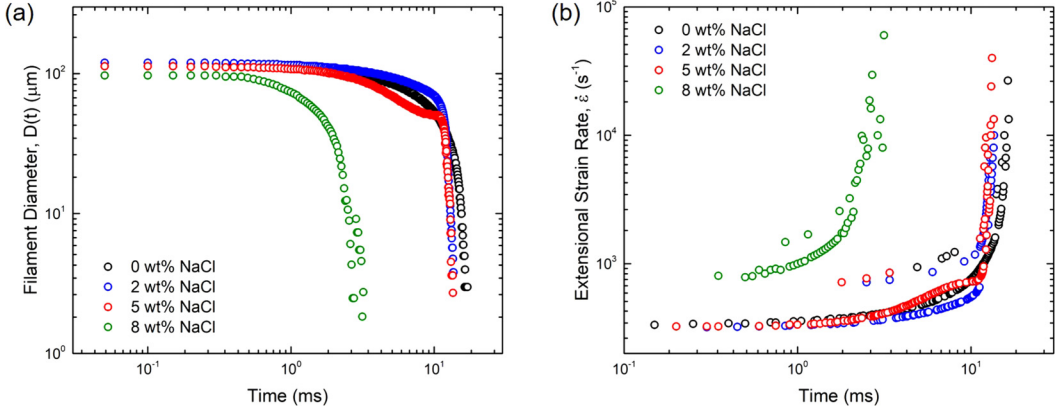


FIG. 6. (a) Filament thinning of the 1 wt% MC150 solution at varying concentrations of NaCl with time. Measurements shown here are taken from a single point in the microfluidic cross-slot channel at 20 000 fps. (b) Calculated extensional strain rate of each 1 wt% MC150 solution with time. The strain rate drastically increases toward the end of the filament-thinning process.

The extensional viscosity of the silicone oil, $\eta_{e,oil}$, can be found using the Trouton ratio, where the extensional viscosity is three times the shear viscosity [58,59]. The calculated extensional viscosity is 0.165 Pa s at 23 °C from cone and plate measurements. The extensional strain rate of the oil, $\dot{\epsilon}_{oil}$, can be approximated using the strain rate from the cross region found by dividing the volumetric flow rate of the oil by the product of the square of the channel width by the channel height [19,60]. However, since the filament itself occupies a portion of the width and height, the extensional strain rate of the oil can be calculated with the following relationship:

$$\dot{\epsilon}_{oil} = \frac{U_{oil}}{W - D(t)} = \frac{Q_{oil}/[HW - \pi(\frac{D(t)}{2})^2]}{W - D(t)}, \quad (4)$$

where U_{oil} is the cross-sectional velocity of the silicone oil, W is the channel width, H is the channel height, $D(t)$ is the filament diameter with time determined by image analysis, and Q_{oil} is the volumetric flow rate of the silicone oil (see Table I). The thinning filament can be thought of as cylindrical in shape as it is unconfined below the channel height, therefore the cross-sectional area is circular. Fig. S8 in the Supplemental Material [43] shows that the centerline velocity of the confined, leading droplet increases with increasing volumetric flow rate of the silicone oil as shown in Table I.

To determine the drag force and ultimately the axial stress due to drag on the overall stress balance across the thinning filament, the confined nature of the droplet must be considered. Although all experiments occur in the $Re < 1$ regime, Stokes' drag is not a good approximation to use here as the confined nature of the leading droplet resembles a “pancake” rather than a sphere. The pancake geometry of the leading droplet is assumed here because in all cases, the diameter of the leading droplet is greater than the channel height of 120 μm (ranging from 125 μm at the smallest to 195 μm at the largest). In cases like these with a confined droplet where the radius of the droplet is larger than the channel height, the pressure drag will dominate over viscous drag, and for a fully confined case, there is no viscous drag contribution [57,61,62]. The pressure drag force component can be expressed as

$$F_{drag} = \frac{24\pi\eta_{s,oil}U_rR^2}{H}, \quad (5)$$

where F_{drag} is the pressure drag force specifically for a confined pancake droplet, $\eta_{s,oil}$ is the shear viscosity of the silicone oil, U_r is the relative velocity between the oil and the leading MC droplet ($U_r = U_{oil} - U_{droplet}$, with droplet velocity $U_{droplet}$ determined with image analysis as shown in

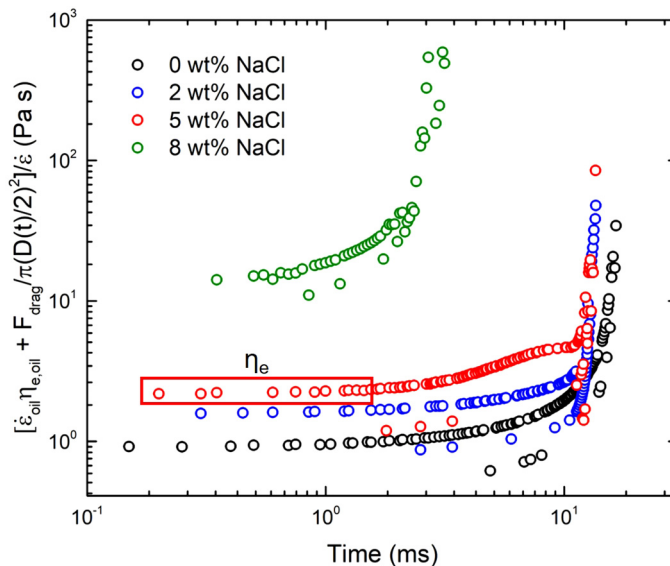


FIG. 7. Stress balance of the outer, continuous oil phase with the inner, dispersed phase of the 1 wt% MC150 solutions with time. The portions of the plot where the quantity is nearly constant with extensional strain rate and time is the flow-driven apparent extensional viscosity, η_e . The red box shows an example of this flow-driven region, and the values for each MC solution are reported in Table I.

Fig. S8 in the Supplemental Material [43]), and R is the projected radius of the leading droplet. To calculate the axial stress, the drag force is then divided by the cross-sectional area of the thinning filament. One caveat here is that the droplets are only partially confined because for a fully confined case, $R/H > 4$ [63]. Therefore, the true drag force and resultant extensional viscosity may be slightly modified as a result.

The quantity $([\eta_{e,oil}\dot{\epsilon}_{oil} + F_{drag}/(\pi(\frac{D(t)}{2})^2)]/\dot{\epsilon})$, which is a rearranged expression from Eq. (3) and shares the same units as extensional viscosity, was calculated for all MC solutions as a function of time, and a representative set of results is shown in Fig. 7. In the region where this quantity is nearly constant with time, and therefore where the extensional strain rate of the MC is also nearly constant with time, the values can be averaged to determine the flow-driven apparent extensional viscosity [20]. The average flow-driven extensional viscosities are shown with 95% confidence intervals in Table I, and they increase from 0.947 ± 0.005 , 1.62 ± 0.01 , 2.7 ± 0.4 , and 15.1 ± 0.6 Pa s as the concentration of NaCl increases from 0, 2, 5, to 8 wt%, respectively. These results are comparable to results obtained by Micklavzina *et al.* [44] using pressure drop measurements in a hyperbolic microchannel. The increase in extensional viscosity by an order of magnitude from 0 to 8 wt% NaCl is attributed to the formation of fibrils in the solution with NaCl. This effect was also seen in CaBER studies of higher molecular weight MC530 [42].

Prior studies using CaBER with MC solutions and the filament stretching technique used here with other polymer solutions show that the extensional viscosity increases above a certain extensional strain rate due to polymer chains aligning and elongating with the direction of the extensional flow field [20,42]. However, the extensional strain rates that those studies accessed were much smaller (e.g., up to approximately 50 s^{-1} from Arratia *et al.* [20]) than the extensional strain rates accessed by this study and by Micklavzina *et al.* [44] (e.g., up to approximately $10,000 \text{ s}^{-1}$). To quantify the relationship between the extensional and shear viscosities, the apparent Trouton ratio was calculated considering uniaxial extensional flow using the following equation:

$$Tr = \frac{\eta_e(\dot{\epsilon}_H)}{\eta_s(\dot{\epsilon}_H\sqrt{3})}, \quad (6)$$

where the extensional viscosity, η_e , and the shear viscosity, η_s , are evaluated at the Hencky strain rate, $\dot{\varepsilon}_H$, and the shear rate equivalent to $\dot{\varepsilon}_H\sqrt{3}$. Approximating the thinning filament as cylindrical, the Hencky strain, ε_H , can be calculated using,

$$\varepsilon_H = 2 \ln \left(\frac{D_0}{D(t)} \right), \quad (7)$$

where D_0 is the initial filament diameter, and the differential at different time points can be used to calculate the Hencky strain rate from the Hencky strain values [64,65].

The apparent Trouton ratios calculated using Eqs. (6) and (7), which are shown in Table I, were found to be 26.9 ± 0.3 , 40.5 ± 0.3 , 56 ± 13 , and 271 ± 35 for 0, 2, 5, and 8 wt% NaCl, respectively. Trouton ratios larger than 3 for non-Newtonian fluids such as the MC solutions tested here are generally expected due to molecular stretching of the polymer chains in stronger extensional flow fields compared to weaker molecular stretching in shear flows. The calculated values of the apparent Trouton ratios can vary over orders of magnitude depending on the strain and strain rates in the experiments as well as the identity and concentration (i.e., how entangled are the chains) of the polymer. Indeed, dilute solutions of linear polymers can reach Trouton ratios several orders of magnitude above the Newtonian limit of 3 [66], whereas branched polymer melts [67] or entangled polymer solutions [68] can exhibit more modest Trouton ratios. The values for the apparent Trouton ratio calculated for the MC150 solutions are within the expected range, if perhaps on the higher end of the expected range, for entangled polysaccharide solutions. A series of studies by Róžańska *et al.* [69,70] measured Trouton ratios between ~ 10 to ~ 100 at similar extensional strain rates for entangled solutions of guar gum and xanthan gum among others.

One should note that the extensional strain rate using the filament thinning device in this study is fixed by the ratio of the volumetric flow rates of the dispersed and continuous phases. Further studies would be needed to explore how the extensional viscosity would depend on strain rate. While this could result in commonly observed extensional thickening, it is also possible to expect extensional thinning seen with similar MC solutions [44] and other entangled and branched polysaccharide systems [70–74]. From this study of the extensional properties of MC solutions, the presence of fibrils continues to have a major effect on the flow-driven apparent extensional viscosity even for low viscosity, weakly elastic MC solutions whose extensional viscosities cannot be measured using traditional macroscale techniques.

IV. CONCLUSION

This study has shown that the flow-drive apparent extensional viscosity of low molecular weight and low viscosity MC solutions can be determined using a flow-focusing microfluidic device at room temperature, with values comparable to another study utilizing microchannels to elucidate extensional viscosity. The order of magnitude increase in apparent extensional viscosity from 0.947 to 15.1 Pa s as the NaCl concentration increased from 0 to 8 wt% was attributed to the presence of a fibrillar MC network in solution at room temperature. The presence of a fibrillar network that forms because of the addition of NaCl to the solution was confirmed by cryo-TEM and shear rheology experiments, corroborating prior studies using macroscale techniques to determine extensional viscosity. This technique provides the opportunity to study extensional viscosity of solutions with lower viscosities and utilizes higher extensional strain rates than are accessible with other commercial techniques, including the CaBER.

ACKNOWLEDGMENTS

This work was supported by the National Science Foundation (NSF) through the University of Minnesota MRSEC under Awards No. DMR-1420013 and No. DMR-2011401. The cryo-TEM images were recorded in the Characterization Facility, University of Minnesota, which receives partial support from the NSF through the MRSEC program under Award No. DMR-1420013. Part

of this work was carried out in the College of Science and Engineering Polymer Characterization Facility, University of Minnesota, which has received capital equipment funding from the NSF through the UMN MRSEC under Award No. DMR-1420013. Portions of this work were conducted in the Minnesota Nano Center, which is supported by the National Science Foundation through the National Nano Coordinated Infrastructure Network (NNCI) under Award No. ECCS-2025124. A.M. and M.C. were each supported through an NSF Graduate Research Fellowship. A.M. would like to thank Dr. Yun Chen, Dr. Benjamin Micklavzina, and Dr. Shweta Narayan for the helpful discussions.

-
- [1] C. G. G. Zehev Tadmor and C. G. Gogos, *Principles of Polymer Processing*, 2nd ed. (John Wiley & Sons, Inc., Hoboken, NJ, 2006).
 - [2] O. A. Basaran, H. Gao, and P. P. Bhat, Nonstandard inkjets, *Annu. Rev. Fluid Mech.* **45**, 85 (2013).
 - [3] G. H. McKinley, Visco-elasto-capillary thinning and break-up of complex fluids, *Rheol. Rev.*, 1 (2005).
 - [4] G. H. McKinley and T. Sridhar, Filament stretching rheometry of complex fluids, *Annu. Rev. Fluid Mech.* **34**, 375 (2002).
 - [5] H. Fong, I. Chun, and D. H. Reneker, Beaded nanofibers formed during electrospinning, *Polymer* **40**, 4585 (1999).
 - [6] R. H. Fernando, L. L. Xing, and J. E. Glass, Rheology parameters controlling spray atomization and roll misting behavior of waterborne coatings, *Prog. Org. Coat.* **40**, 35 (2000).
 - [7] A. R. Metcalf, H. C. Boyer, and C. S. Dutcher, Interfacial tensions of aged organic aerosol particle mimics using a biphasic microfluidic platform, *Environ. Sci. Technol.* **50**, 1251 (2016).
 - [8] H. C. Boyer and C. S. Dutcher, Atmospheric aqueous aerosol surface tensions: Isotherm-based modeling and biphasic microfluidic measurements, *J. Phys. Chem. A* **121**, 4733 (2017).
 - [9] S. Narayan, D. B. Moravec, B. G. Hauser, A. J. Dallas, and C. S. Dutcher, Removing water from diesel fuel: Understanding the impact of droplet size on dynamic interfacial tension of water-in-fuel emulsions, *Energy Fuels* **32**, 7326 (2018).
 - [10] A. Schröder, J. Sprakel, K. Schroën, J. N. Spaen, and C. C. Berton-Carabin, Coalescence stability of Pickering emulsions produced with lipid particles: A microfluidic study, *J. Food Eng.* **234**, 63 (2018).
 - [11] L. A. Chacon Orellana and J. Baret, Rapid stabilization of droplets by particles in microfluidics: Role of droplet formation, *ChemSystemsChem* **1**, 16 (2019).
 - [12] V. Sharma, S. J. Haward, J. Serdy, B. Keshavarz, A. Soderlund, P. Threlfall-Holmes, and G. H. McKinley, The rheology of aqueous solutions of ethyl hydroxy-ethyl cellulose (EHEC) and its hydrophobically modified analogue (hmEHEC): Extensional flow response in capillary break-up, jetting (ROJER) and in a cross-slot extensional rheometer, *Soft Matter* **11**, 3251 (2015).
 - [13] B. Keshavarz, V. Sharma, E. C. Houze, M. R. Koerner, J. R. Moore, P. M. Cotts, P. Threlfall-Holmes, and G. H. McKinley, Studying the effects of elongational properties on atomization of weakly viscoelastic solutions using Rayleigh Ohnesorge jetting extensional rheometry (ROJER), *J. Non-Newtonian Fluid Mech.* **222**, 171 (2015).
 - [14] J. Dinic, Y. Zhang, L. N. Jimenez, and V. Sharma, Extensional relaxation times of dilute, aqueous polymer solutions, *ACS Macro Lett.* **4**, 804 (2015).
 - [15] J. Dinic, M. Biagioli, and V. Sharma, Pinch-off dynamics and extensional relaxation times of intrinsically semi-dilute polymer solutions characterized by dripping-onto-substrate rheometry, *J. Polym. Sci. Part B Polym. Phys.* **55**, 1692 (2017).
 - [16] E. Miller, C. Clasen, and J. P. Rothstein, The effect of step-stretch parameters on capillary breakup extensional rheology (CaBER) measurements, *Rheol. Acta* **48**, 625 (2009).
 - [17] C. Clasen, J. P. Plog, W.-M. Kulicke, M. Owens, C. Macosko, L. E. Scriven, M. Verani, and G. H. McKinley, How dilute are dilute solutions in extensional flows? *J. Rheol.* **50**, 849 (2006).
 - [18] C. Clasen, Capillary breakup extensional rheometry of semi-dilute polymer solutions, *Korea-Australia Rheol. J.* **22**, 331 (2010).

- [19] P. E. Arratia, C. C. Thomas, J. Diorio, and J. P. Gollub, Elastic Instabilities of Polymer Solutions in Cross-Channel Flow, *Phys. Rev. Lett.* **96**, 144502 (2006).
- [20] P. E. Arratia, J. P. Gollub, and D. J. Durian, Polymeric filament thinning and breakup in microchannels, *Phys. Rev. E* **77**, 036309 (2008).
- [21] L. E. Rodd, J. J. Cooper-White, D. V. Boger, and G. H. McKinley, Role of the elasticity number in the entry flow of dilute polymer solutions in micro-fabricated contraction geometries, *J. Non-Newtonian Fluid Mech.* **143**, 170 (2007).
- [22] B. Keshavarz and G. H. McKinley, Micro-scale extensional rheometry using hyperbolic converging/diverging channels and jet breakup, *Biomicrofluidics* **10**, 043502 (2016).
- [23] S. J. Haward, M. S. N. Oliveira, M. A. Alves, and G. H. McKinley, Optimized Cross-Slot Flow Geometry for Microfluidic Extensional Rheometry, *Phys. Rev. Lett.* **109**, 128301 (2012).
- [24] F. Del Giudice, S. J. Haward, and A. Q. Shen, Relaxation time of dilute polymer solutions: A microfluidic approach, *J. Rheol.* **61**, 327 (2017).
- [25] C. J. Pipe and G. H. McKinley, Microfluidic rheometry, *Mech. Res. Commun.* **36**, 110 (2009).
- [26] S. L. Anna and G. H. McKinley, Elasto-capillary thinning and breakup of model elastic liquids, *J. Rheol.* **45**, 115 (2001).
- [27] S. L. Anna, N. Bontoux, and H. A. Stone, Formation of dispersions using “flow focusing” in microchannels, *Appl. Phys. Lett.* **82**, 364 (2003).
- [28] T. Chatterjee, A. I. Nakatani, R. Adden, M. Brackhagen, D. Redwine, H. Shen, Y. Li, T. Wilson, and R. L. Sammler, Structure and properties of aqueous methylcellulose gels by small-angle neutron scattering, *Biomacromolecules* **13**, 3355 (2012).
- [29] Y. Xu, C. Wang, K. C. Tam, and L. Li, Salt-assisted and salt-suppressed sol-gel transitions of methylcellulose in water, *Langmuir* **20**, 646 (2004).
- [30] Y. Xu, L. Li, P. Zheng, Y. C. Lam, and X. Hu, Controllable gelation of methylcellulose by a salt mixture, *Langmuir* **20**, 6134 (2004).
- [31] J. R. Lott, J. W. McAllister, S. A. Arvidson, F. S. Bates, and T. P. Lodge, Fibrillar structure of methylcellulose hydrogels, *Biomacromolecules* **14**, 2484 (2013).
- [32] S. A. Arvidson, J. R. Lott, J. W. McAllister, J. Zhang, F. S. Bates, T. P. Lodge, R. L. Sammler, Y. Li, and M. Brackhagen, Interplay of phase separation and thermoreversible gelation in aqueous methylcellulose solutions, *Macromolecules* **46**, 300 (2013).
- [33] J. R. Lott, J. W. McAllister, M. Wasbrough, R. L. Sammler, F. S. Bates, and T. P. Lodge, Fibrillar structure in aqueous methylcellulose solutions and gels, *Macromolecules* **46**, 9760 (2013).
- [34] J. W. McAllister, J. R. Lott, P. W. Schmidt, R. L. Sammler, F. S. Bates, and T. P. Lodge, Linear and nonlinear rheological behavior of fibrillar methylcellulose hydrogels, *ACS Macro Lett.* **4**, 538 (2015).
- [35] J. W. McAllister, P. W. Schmidt, K. D. Dorfman, T. P. Lodge, and F. S. Bates, Thermodynamics of aqueous methylcellulose solutions, *Macromolecules* **48**, 7205 (2015).
- [36] P. W. Schmidt, S. Morozova, P. M. Owens, R. Adden, Y. Li, F. S. Bates, and T. P. Lodge, Molecular weight dependence of methylcellulose fibrillar networks, *Macromolecules* **51**, 7767 (2018).
- [37] I. R. Bruss and G. M. Grason, Topological defects, surface geometry and cohesive energy of twisted filament bundles, *Soft Matter* **9**, 8327 (2013).
- [38] D. M. Hall, I. R. Bruss, J. R. Barone, and G. M. Grason, Morphology selection via geometric frustration in chiral filament bundles, *Nat. Mater.* **15**, 727 (2016).
- [39] D. M. Hall and G. M. Grason, How geometric frustration shapes twisted fibres, inside and out: competing morphologies of chiral filament assembly, *Interface Focus* **7**, 20160140 (2017).
- [40] V. Sethuraman and K. D. Dorfman, Simulating precursor steps for fibril formation in methylcellulose solutions, *Phys. Rev. Mater.* **3**, 055601 (2019).
- [41] P. W. Schmidt, S. Morozova, S. P. Ertem, M. L. Coughlin, I. Davidovich, Y. Talmon, T. M. Reineke, F. S. Bates, and T. P. Lodge, Internal structure of methylcellulose fibrils, *Macromolecules* **53**, 398 (2020).
- [42] S. Morozova, P. W. Schmidt, A. Metaxas, F. S. Bates, T. P. Lodge, and C. S. Dutcher, Extensional flow behavior of methylcellulose solutions containing fibrils, *ACS Macro Lett.* **7**, 347 (2018).

- [43] See Supplemental Material at <http://link.aps.org/supplemental/10.1103/PhysRevFluids.5.113302> for further information regarding rheological measurements and analysis, repeat filament thinning for each sample, and image analysis for filament thinning in region of interest and drag calculations.
- [44] B. L. Micklavzina, A. E. Metaxas, and C. S. Dutcher, Microfluidic rheology of methylcellulose solutions in hyperbolic contractions and the effect of salt in shear and extensional flows, *Soft Matter* **16**, 5273 (2020).
- [45] T. J. Ober, S. J. Haward, C. J. Pipe, J. Soulages, and G. H. McKinley, Microfluidic extensional rheometry using a hyperbolic contraction geometry, *Rheol. Acta* **52**, 529 (2013).
- [46] H. S. Lee and S. J. Muller, A differential pressure extensional rheometer on a chip with fully developed elongational flow, *J. Rheol.* **61**, 1049 (2017).
- [47] T. Funami, Y. Kataoka, M. Hiroe, I. Asai, R. Takahashi, and K. Nishinari, Thermal aggregation of methylcellulose with different molecular weights, *Food Hydrocoll.* **21**, 46 (2007).
- [48] Y. Xia and G. M. Whitesides, Soft lithography, *Annu. Rev. Mater. Sci.* **28**, 153 (1998).
- [49] J. C. McDonald and G. M. Whitesides, Poly(dimethylsiloxane) as a material for fabricating microfluidic devices, *Acc. Chem. Res.* **35**, 491 (2002).
- [50] D. Qin, Y. Xia, and G. M. Whitesides, Soft lithography for micro- and nanoscale patterning, *Nat. Protoc.* **5**, 491 (2010).
- [51] J. Dinic and V. Sharma, Power laws dominate shear and extensional rheology response and capillarity-driven pinching dynamics of entangled hydroxyethyl cellulose (HEC) solutions, *Macromolecules* **53**, 3424 (2020).
- [52] E. Daly and B. R. Saunders, Study of the effect of electrolyte on the swelling and stability of poly(N-isopropylacrylamide) microgel dispersions, *Langmuir* **16**, 5546 (2000).
- [53] A. A. Polotsky, F. A. Plamper, and O. V. Borisov, Collapse-to-swelling transitions in pH- and thermoresponsive microgels in aqueous dispersions: The thermodynamic theory, *Macromolecules* **46**, 8702 (2013).
- [54] O. Zavgorodnya, V. Kozlovskaya, X. Liang, N. Kothalawala, S. A. Catledge, A. Dass, and E. Kharlampieva, Temperature-responsive properties of poly(N-vinylcaprolactam) multilayer hydrogels in the presence of Hofmeister anions, *Mater. Res. Express* **1**, 035039 (2014).
- [55] Y. Amarouchene, D. Bonn, J. Meunier, and H. Kellay, Inhibition of the Finite-Time Singularity during Droplet Fission of a Polymeric Fluid, *Phys. Rev. Lett.* **86**, 3558 (2001).
- [56] M. S. N. Oliveira and G. H. McKinley, Iterated stretching and multiple beads-on-a-string phenomena in dilute solutions of highly extensible flexible polymers, *Phys. Fluids* **17**, 071704 (2005).
- [57] R. Dangla, S. Lee, and C. N. Baroud, Trapping Microfluidic Drops in Wells of Surface Energy, *Phys. Rev. Lett.* **107**, 124501 (2011).
- [58] C. W. Macosko, *Rheology: Principles, Measurements, and Applications* (Wiley-VCH, Berlin, 1994).
- [59] F. T. Trouton, On the coefficient of viscous traction and its relation to that of viscosity, *Proc. R. Soc. A* **77**, 426 (1906).
- [60] G. Juarez and P. E. Arratia, Extensional rheology of DNA suspensions in microfluidic devices, *Soft Matter* **7**, 9444 (2011).
- [61] D. A. Sessoms, M. Belloul, W. Engl, M. Roche, L. Courbin, and P. Panizza, Droplet motion in microfluidic networks: hydrodynamic interactions and pressure-drop measurements, *Phys. Rev. E* **80**, 016317 (2009).
- [62] S. A. Vanapalli, A. G. Banpurkar, D. Van Den Ende, M. H. G. Duits, and F. Mugele, Hydrodynamic resistance of single confined moving drops in rectangular microchannels, *Lab Chip* **9**, 982 (2009).
- [63] P.-T. Brun, M. Nagel, and F. Gallaire, Generic path for droplet relaxation in microfluidic channels, *Phys. Rev. E* **88**, 043009 (2013).
- [64] E. Greiciunas, J. Wong, I. Gorbatenko, J. Hall, M. C. T. Wilson, N. Kapur, O. G. Harlen, D. Vaddillo, and P. Threlfall-Holmes, Design and operation of a Rayleigh Ohnesorge jetting extensional rheometer (ROJER) to study extensional properties of low viscosity polymer solutions, *J. Rheol.* **61**, 467 (2017).
- [65] M. D. Torres, B. Hallmark, D. I. Wilson, and L. Hilliou, Natural Giesekus fluids: Shear and extensional behavior of food gum solutions in the semidilute regime, *AIChE J.* **60**, 3902 (2014).
- [66] S. L. Anna, G. H. McKinley, D. A. Nguyen, T. Sridhar, S. J. Muller, J. Huang, and D. F. James, An interlaboratory comparison of measurements from filament-stretching rheometers using common test fluids, *J. Rheol.* **45**, 83 (2001).

- [67] H. Münstedt and H. M. Laun, Elongational properties and molecular structure of polyethylene melts, *Rheol. Acta* **20**, 211 (1981).
- [68] R. G. Larson and P. S. Desai, Modeling the rheology of polymer melts and solutions, *Annu. Rev. Fluid Mech.* **47**, 47 (2015).
- [69] S. Róžańska, L. Broniarz-Press, J. Róžański, P. T. Mitkowski, M. Ochowiak, and S. Woziwodzki, Extensional viscosity of o/w emulsion stabilized by polysaccharides measured on the opposed-nozzle device, *Food Hydrocoll.* **32**, 130 (2013).
- [70] S. Róžańska, *Advances in Food Rheology and Its Applications* (Woodhead Publishing, Cambridge, UK, 2017).
- [71] D. M. Jones, K. Walters, and P. R. Williams, On the extensional viscosity of mobile polymer solutions, *Rheol. Acta* **26**, 20 (1987).
- [72] M. D. Torres, B. Hallmark, and D. I. Wilson, Effect of concentration on shear and extensional rheology of guar gum solutions, *Food Hydrocoll.* **40**, 85 (2014).
- [73] S. L. Wingstrand, N. J. Alvarez, Q. Huang, and O. Hassager, Linear and Nonlinear Universality in the Rheology of Polymer Melts and Solutions, *Phys. Rev. Lett.* **115**, 078302 (2015).
- [74] S. Róžańska, K. Verbeke, J. Róžański, C. Clasen, and P. Wagner, Capillary breakup extensional rheometry of sodium carboxymethylcellulose solutions in water and propylene glycol/water mixtures, *J. Polym. Sci. Part B Polym. Phys.* **57**, 1537 (2019).